Available online at www.sciencedirect.com
SCIENCE DIRECT
Polymer 46 (2005) 10339–10354
polymer
www.elsevier.com/locate/polymer

Influence of molecular parameters on high-strain deformation of polyethylene in the plane-strain compression. Part II. Strain recovery

Z. Bartczak*

Polymer Physics, Centre of Molecular Macromolecular Studies, Polish Academy of Sciences, Sienkiewicza 112, 90 363 Lodz, Poland

Received 25 April 2005; received in revised form 13 July 2005; accepted 29 July 2005
Available online 24 August 2005

Abstract

Deformation and recovery behavior of the series of polyethylenes and ethylene-based copolymers with various molecular architecture and a broad range of molecular mass and its distribution, was studied. Due to the differences in molecular characteristic, this series exhibited a relatively broad range of crystallite sizes as well as crystallinity level, varying from 10 wt% up to more than 70 wt%.

The samples were subjected to high-strain compression in the plane-strain conditions, above the true strain of 2. The strain recovery in the entire strain range was studied experimentally. The amount of recovered strain as well as its rate were related to molecular parameters of the material. The obtained results confirmed the common deformation scheme with four invariant cross-over points related to the activation of subsequent deformation mechanisms, including crystal fragmentation and erosion of the molecular network by chain disentanglements. This scheme was found in the past for tensile deformation. The influence of molecular network of entangled chains within amorphous component on the deformation and recovery behavior was discussed.

Keywords: Polyethylene; Strain recovery; Chain entanglements

1. Introduction

Plastic deformation of semicrystalline polymers was extensively studied in the past decades with particular attention given to the deformation of the crystalline component, which resulted in a broad knowledge of the mechanisms employed [1–3]. However, there is considerably less understanding of the role of an amorphous component in the deformation sequence and interactions between adjacent layers of crystalline and amorphous component, which are intimately connected by covalent bonds and must deform simultaneously due to continuity condition.

An amorphous component consists of highly entangled chains forming a continuous molecular network. Additionally, it contains a certain fraction of tie-molecules, which connect neighboring lamellae and are able to transmit stress between them [4,5]. The entanglements, tie-molecules and crystallites adjacent to the amorphous layers constitute physical cross-links of this network. The network should manifest itself in high reversibility of the deformation, which in fact, is frequently observed experimentally.

Recently, Strobl et al. [6–11] focused on these aspects of the deformation of semicrystalline polymers, which are related to the presence of the molecular network. They studied the tensile deformation and recovery behavior of several semicrystalline polymers, including a series of polyethylenes [6,9] and found a quite simple general deformation scheme, which was followed by all polymers studied. The main feature of this universal behavior is that the process of deformation is controlled by the strain rather than stress. Along the true stress–true strain curves the differential compliance, recovery behavior as well as the crystalline texture change simultaneously at well defined points. Four characteristic points were identified and ascribed to:

(A) The onset of isolated inter- and intralamellar slip processes (true strain, $e \sim 0.025$).
(B) The change into a collective activity of slips (macroscopic yield point, $e \sim 0.1$).

* Tel.: +48 42 6803237; fax: +48 42 6847126.
E-mail address: bartczak@bilbo.cbmm.lodz.pl.

0032-3861/$ - see front matter © 2005 Elsevier Ltd. All rights reserved.
doi:10.1016/j.polymer.2005.07.096

(C) The beginning of crystallite fragmentation and fibril formation ($e \sim 0.6$).
(D) The onset of chain disentanglement ($e \sim 1.0$).

The critical strains at which these points take place were found invariant over various strain rates and drawing temperatures [7,10], as well as crystallinity of a polymer [6,8,10]. In contrast, the corresponding stresses varied significantly with crystallinity as well as with strain rate or temperature of deformation. The invariance of critical strains, i.e. the strain control of the deformation behavior, implies that the strain can be considered as homogeneous in a semi-crystalline polymer upon its deformation. Active crystallographic slips supported by interlamellar shear modes offer sufficient degrees of freedom to achieve that [2,3].

Upon deformation at temperature above T_g the load is transmitted by two interpenetrating networks: The skeleton of crystallites and the rubber-like entanglement network of the amorphous regions. However, with an advance of the deformation process, the respective weights change. At low strain, the highly compliant amorphous phase can deform considerably more rapidly than the crystalline phase, yet its contribution to the plastic deformation is limited due to constraints imposed by adjacent crystals through chains crossing crystal–amorphous interface (tie-molecules, cilia and loose loops, entangled with other chains), and its principal role is to transmit load to and between crystalline lamellae [3,4,12,13]. However, at high strain the increasing network forces become dominant, which manifests itself in a strong amorphous phase orientation hardening and consequently macroscopic strain hardening [13]. Correspondingly, the yield point (B) is a property of the crystalline skeleton, which above that point is continuously readjusted by operating slip systems. Much more compliant amorphous layers, intimately connected to crystallites follow the changes of crystallites orientation undergoing interlamellar shear up to point C, where stresses generated in the stretched network of amorphous chains become high enough to trigger fragmentation of adjacent crystallites [6]. Finally, at high strains, deformation behavior becomes dominated by forces produced by the stretched entanglement network.

High strain deformation and recovery behavior of other polymers such as PET, PBT or nylon-6 were also studied by other authors [14–21]. Their findings are generally consistent with the deformations scheme proposed by Strobl et al. [6].

In the companion paper [22] (Part I of this study) we have reported the study of the deformation behavior of a series of samples of polyethylene and ethylene-based copolymers, covering a broad range of molecular mass and chain architecture. These samples demonstrated a notable variation in the amount and properties of the amorphous phase, yet similar structure of the crystalline component and similar supermolecular structure. Special attention was given in this study to the role of the amorphous phase as well as its topological structure in the high-strain deformation behavior. The mechanical response was correlated with the properties of the molecular network within amorphous component, which appeared to be influenced markedly by the molecular parameters, like molecular weight and architecture of the chains [22]. Properties of this network control the stress–strain behavior, especially in the range of high-applied strains. This paper presents supplementary results of investigations of the post-deformation recovery process of the same materials. These results allowed us to analyze the deformation behavior in relation to the deformation scheme proposed by Strobl et al. [6].

Although most of the deformation studies performed in the past employed uniaxial drawing, we decided to implement plane-strain compression for our studies in order to avoid any side-effects that usually accompany tensile deformation, as necking instability or cavitation phenomena. Such phenomena obscure seriously the real micro-mechanisms involved in the deformation process. In contrast, the deformation in plane-strain compression mode proceeds homogeneously, without any instability, while kinematically it is similar to tension, leading to the axial flow of the polymer in the direction perpendicular to a compressive load [12]. Suppression of any cavitation phenomena due to compressive stress components results in deformation to the strain and stress usually reasonably higher than in tension, practically without a premature fracture of the sample. This allows to study the deformation behavior to higher strains and to avoid any unwanted phenomena, which are inessential from the point of view of view of the real mechanisms involved.

2. Experimental

2.1. Materials and sample preparation

Materials used in this study were the samples of various grades of commercial polyethylene, including five linear high-density polyethylenes of various molecular mass, (HDPE, samples H-1 to H-5) two samples of ultra-high molecular mass polyethylene (UHMWPE, samples U-1 and U-2), five conventional branched polyethylenes of different branching level and molecular mass (LDPE, samples L-1 to L-5) and four copolymers of ethylene with various contents of butene-1 or octene-1 comonomer (linear low density polyethylenes, LLDPE and ethylene–octene-1 elastomers, samples LL-1, LL-2, E-1 and E-2, respectively). The characteristic of the polymers is given in the companion paper (Part I) [22].

Samples, in the form of 50×50 mm^2 plates, 4 mm thick, were prepared by compression molding. The compressed plates were solidified by fast cooling in iced water. Specimens of the size desired for particular experiments

were machined out from these plates. In order to minimize differences in the structure of samples due to differences in crystallization conditions, all samples were prepared according to the identical procedure, at the same thermal conditions, which resulted in the formation of similar supermolecular structure of investigated materials. Details of the preparation procedure are described in Ref. [22].

2.2. Characterization

2.2.1. SAXS

A lamellar structure of raw and deformed samples was probed by 2D small angle X-ray scattering (2D SAXS). A 1.1 m long Kiessig-type camera was equipped with a tapered capillary (XOS), a pinhole collimator and an imaging plate as a detector (Fuji). The camera was coupled to a X-ray generator (sealed-tube, fine point Cu K_α filtered source operating at 50 kV and 40 mA; Philips). Exposed imaging plates were read with a Phosphor-Imager SI system (Molecular Dynamics).

2.2.2. TEM

Observations of ultra-thin sections of the selected samples were performed with a transmission electron microscope (TESLA BS500). The samples were stained with chlorosulfonic acid prior to sectioning, according to the procedure of Kanig [23]. Ultra-thin sections were produced with an ultramicrotome (TESLA) equipped with a freshly prepared glass knife.

2.3. Deformation and recovery experiments

Plane-strain compression was chosen as a deformation mode throughout this study. The plane-strain compression tests were performed using the loading frame of 5 ton capacity (Instron, Model 1114) and a compression tool of the type of a channel-die equipped with load and strain gauges. Two compression tools of different size and geometry were used in this study. Both are shown schematically in Fig. 1. The first tool (Fig. 1(a)) was a conventional deep channel-die [24,25], with a channel 3.85 mm wide (along constrained direction, CD), 50 mm long (along flow direction, FD) and 60 mm deep (along loading direction, LD), allowing samples up to 40 mm high (i.e. dimension along LD) to be compressed with that die. The second tool (Fig. 1(b)) was a set of a lower die with a wide rectangular channel cut across the die and an upper plunger fitting the channel in the lower die. The channel in the lower die was 15 mm wide (i.e. along CD) 6 mm long (along FD), and 6 mm deep (along LD). To provide a precise position and guidance of the plunger against the lower die, a special fixture, shown schematically in Fig. 1(b) with a broken line, was used.

The advantage of a deep channel-die is tht the samples produced by compression in such a die are relatively large, so that the structure and orientation produced by plastic

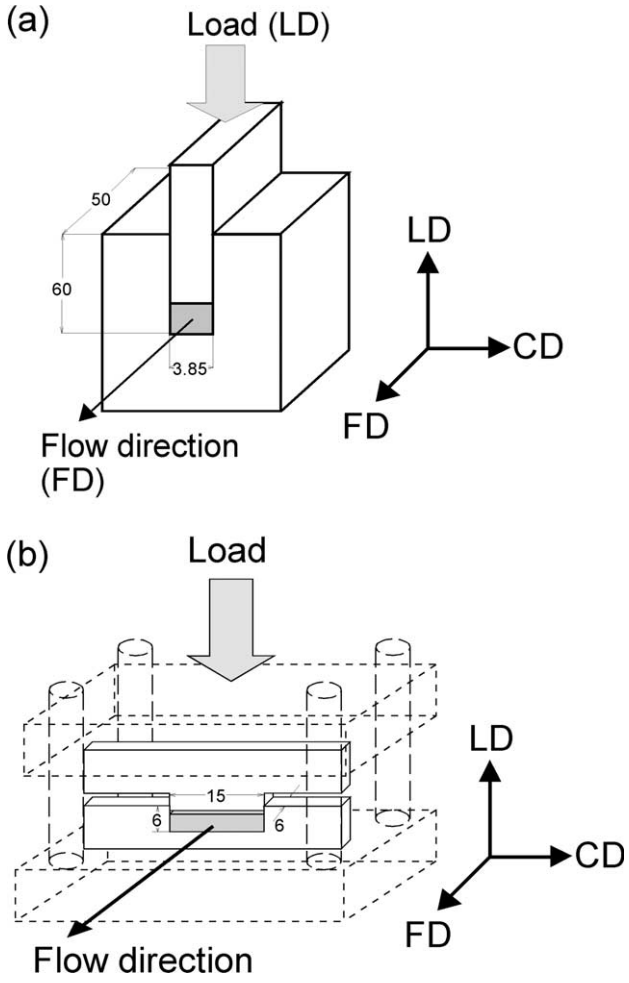

Fig. 1. Deformation tools used for plane-strain compression: (a) Deep channel die, (b) small die. The compressed sample is marked gray. In (b) the guidance fixture is shown with broken line. Dimensions given in mm.

deformation as well as the macroscopic recovery behavior could be studied easily. On the other hand, due to large lateral surface area of the sample, friction forces between the sample and die could not be neglected, which resulted in overestimation of the stress. This was the case even when the sample and the die were adequately lubricated prior to compression.

Compression in a smaller, wide channel-die does not generate so much friction since the ratio of lateral surface to the sample volume is smaller than in the deep channel-die. Therefore, when the sample is properly lubricated, the friction component is relatively small and does not modify significantly the recorded stress–strain curves. For this reason we used this tool for most of compression experiments for which the stress–strain curves were essential as well as for part of strain recovery experiments.

The size of specimens used in a deep channel-die compression was $3.85 \times 50 \times 40$ mm^3 (along CD, FD and LD, respectively) while those compressed in a small die were $15 \times 6 \times 4$ mm^3 (CD × FD × LD).

All deformation experiments were performed at a constant speed of the crosshead of the loading frame. The speed of the crosshead was set to give the initial deformation rate of 5% per min ($8.3\times10^{-4}\,s^{-1}$) for both sample sizes. All compression tests described in this paper were performed at room temperature.

Two types of deformation experiments were performed. One was a continuous compression with a constant speed in a single run up to the desired strain. After reaching that strain the specimen was unloaded and immediately withdrawn from a die to allow its unconstrained recovery.

The second type of deformation experiment was a 'step-cycle' test [6] using a small die. In this test, the specimen was deformed first to some pre-selected strain (step), then the crosshead was stopped and retracted with the same speed as on compression until load reached back the zero value. At this point, the direction of the crosshead was reverted again and the sample was compressed (cycle), now to another pre-selected strain, higher than that reached in a previous step. Next, the specimen was unloaded once more and the entire cycle was repeated. In such a stepwise manner the samples were deformed up to high strains, comparable to strains applied to the same material in continuous loading experiments. Measurements of sample dimensions demonstrated that in the small die, due to a relatively small contribution of friction, the partial recovery of the strain in each cycle was almost undisturbed as compared to the recovery in free, unconstrained conditions.

The post-deformation behavior of continuously loaded specimens was monitored after sample unloading and withdrawal from a die. The specimen length (i.e. along FD), width (along CD) and height (along LD) were measured repeatedly over a period of time, until no further change of the sample dimensions was detected. This deformation recovery period extended in several cases over a month after specimen unloading. The respective recovered part of the strain was calculated from the measured changes of specimen dimensions.

In a separate experiment the samples, already recovered at room temperature over a long period of time, were slowly heated up in an oil bath to the temperature approaching melting point of the polymer studied. An oil immersion was used to reduce any external constraints during that strain recovery process. After 10 min of annealing, the samples were cooled down and then their final dimensions were measured and recovered strains calculated.

3. Results

3.1. Recovery behavior

The stress–strain behavior of studied polyethylene and copolymer samples was described and analyzed in Part I [22]. It was found that the deformation of studied polyethylenes and copolymers in plane-strain compression at room temperature proceeded homogeneously up to high strains, exceeding the compression ratio of 10 (true strain well above of $e=2$). The deformation to high strain led to an intense strain hardening resulting in a very high stress, frequently exceeding 500 MPa. Such an intense strain hardening appeared to be related to deformation of the molecular network of entangled chains within the amorphous component. The stress response of particular samples was found to correlate with the properties of the molecular network, controlled primarily by the molecular weight of a respective polymer and by the architecture of its chain [22].

More insight in the deformation process can be delivered by recovery experiments, described in this paper. The first recovery test carried out was the step-cycle test, illustrated in Fig. 2. In this test, the stress first grows during the stepwise strain increment and then follows a hysteresis loop during an unloading–reloading cycle. For comparison, the true stress–true strain curve measured for continuous loading in an uninterrupted run of another specimen of the same polymer is also presented. It can be seen that the stress developed in the stepwise compression always approaches that observed in the continuous loading. Such a behavior was observed in all samples studied, although some deviations were observed sporadically for highly crystalline HDPE samples in the range of very high strains, well within the strain hardening region (true strain, $e\sim1.5$–1.7). The overlapping of the envelope of the step-cycle curve with the continuous curve demonstrates clearly that no irreversible structure changes or flow occurs during the cycling time, at least to the true strain of approx. 1.5. It evidences also that the actual state of the deformed material depends only on the strain applied, and does not depend on the mechanical history of the sample. This supports the view that plastic deformation of semicrystalline polymer is a strain-controlled process [6]. Another feature of the step-cycle experiments was that similarly to the continuous compression tests, no trace of cavitation of the material at any stage of its deformation or recovery was observed.

A qualitative comparison of various samples tested in the step-cycle experiment shows that the strain recovery, occurring on unloading, is relatively small in highly crystalline linear PE and then increases with an increasing contribution of the amorphous component for other samples.

In the step-cycle test the total strain applied to the sample can be split into two parts: A recoverable one, e_{r0}, describing the strain associated with the cycle, and a second one—the strain remaining in the sample at the moment of its unloading, e_{p0} [6,19]:

$$e = e_{r0} + e_{p0} \tag{10}$$

After Strobl et al. [6], we can call these strain components as cyclic and base strains, respectively. The strain amplitude of each cycle yields recoverable part of the

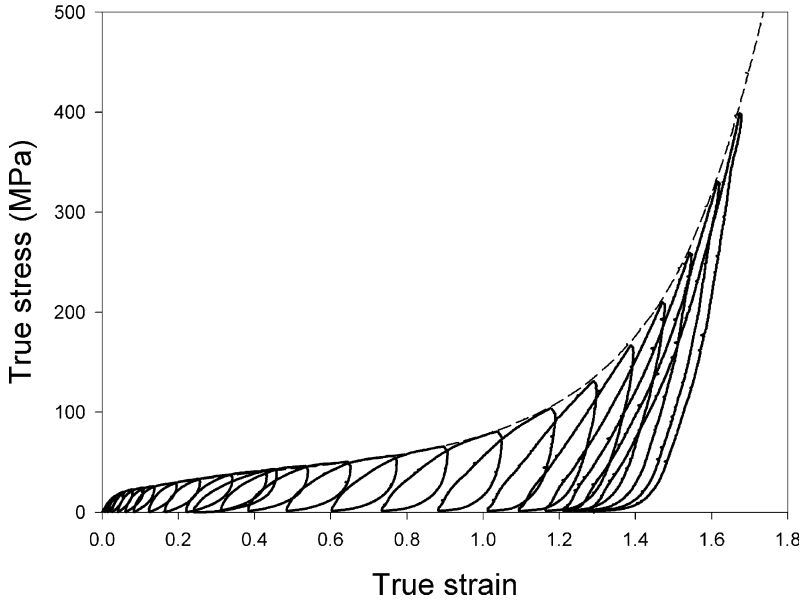

Fig. 2. Exemplary plot illustrating the step-cycle compression experiment, obtained for sample U-2 (solid line). For comparison a dashed line shows the stress–strain behavior of the same material compressed in a continuous manner.

strain, e_{r0}. That strain component can be further divided into instantaneous elastic recovery and a time-dependent part [19]. One should note that the recovery observed in the step-cycle experiment can be far from completion due to a limited time scale of the unloading stage. Therefore, the step-cycle test can provide information only on the fastest part of the recovery process characterized by the shortest relaxation times. For the same reason the base strain component, e_{p1}, can be considered as a permanent one only in the time scale of this particular experiment.

Fig. 3 shows a few exemplary results of the decomposition of the strain into the recoverable (cyclic, e_{r0}) and remaining (base, e_{p0}) strain on the basis of the data collected

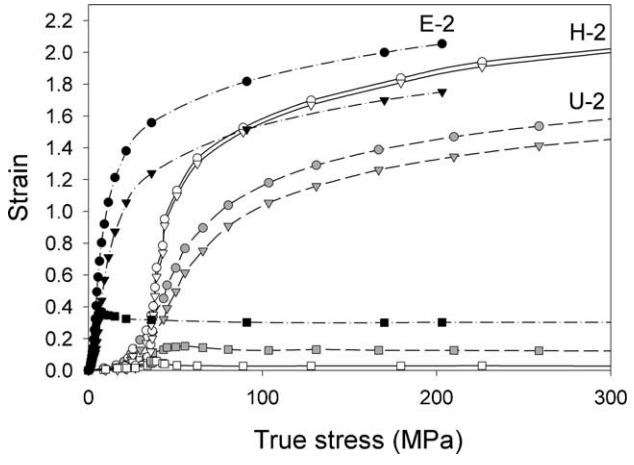

Fig. 3. Strain decomposed into recoverable (cyclic) and remaining (base) components on the basis of the data collected in step-cycle recovery tests plotted as a function of true stress. Circles, triangles and squares represent total strain, base strain and recovered strain, respectively. Open symbols are used for H-2 linear homopolymer, gray for U-2 UHMWPE and black for E-2 copolymer.

in the step-cycle deformation tests. This figure presents strain components as determined for highly crystalline linear polyethylene H-2, exhibiting the lowest recovery in the series, U-2 UHMWPE sample of moderate crystallinity and strain recovery and a very low crystallinity elastomeric sample E-2 exhibiting the highest strain recovery. The total strain along with its two components were plotted as a function of the applied true stress. One can see that for a given polymer, the recovery (cyclic) strain, e_{r0}, after passing a low maximum remains practically constant over a very broad range of stress, which indicates clearly that recovery does not depend on the stress level.

Fig. 4 presents the same data of recoverable (cyclic, e_{r0}) and remaining (base, e_{p0}) strain components determined for investigated samples, now plotted as a function of the applied strain. Curves of the cyclic strain vs. applied strain, shown in Fig. 4(a), have a similar shape for all polymers studied, with a low and broad maximum centered around the strain of approx. 0.6. The second common feature of these curves is a plateau region of lower recovered strain, extending in the range of high applied strain, above $e \sim 1.0$–1.2. Taking into account a very broad range of the molecular characteristic and crystallinity of the studied polymers, these common features of all curves provide evidence that the recovery behavior is controlled principally by the applied strain.

The evolution of the remaining (base) strain is presented in Fig. 4(b). For clarity, only two extreme samples: Highly crystalline H-1 and very low crystalline E-2, are shown. Other curves have similar shape to the presented ones and fall between these two. A straight solid line with a slope of 1, representing the behavior of a perfect plastic material is also plotted for reference. At the beginning of the deformation process, up the strain of approx. 0.6, the e_{p0}

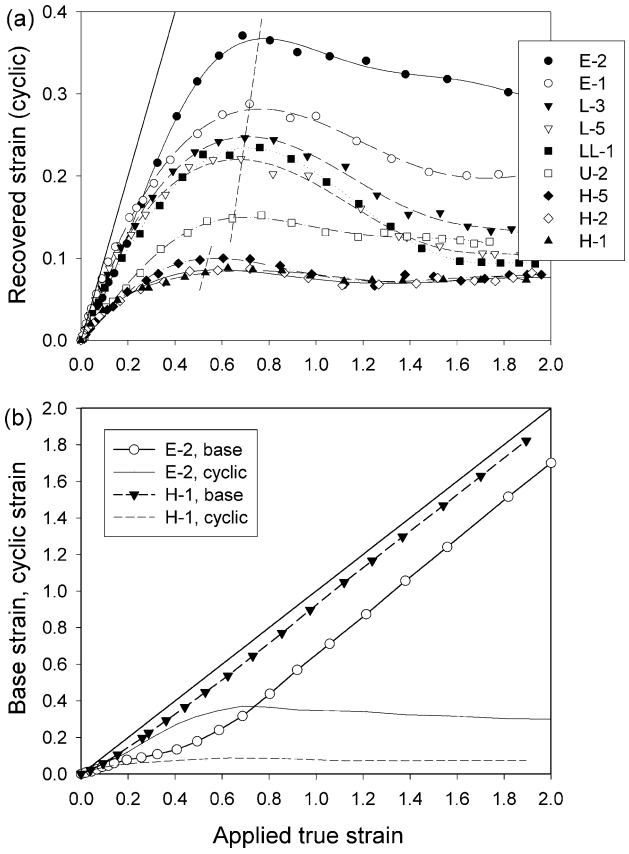

Fig. 4. Dependencies of recoverable (a) and base strains (b) on the applied strain in samples indicated in the legend. Straight line of the unit slope in (a) illustrates an ideal elastic behavior, while that in (b) represents an ideal plastic. For clarity, in (b) only extreme curves of E-2 and H-1 are presented. For comparison the respective recovered strains were replotted from (a).

strain component (base), i.e. the strain permanent in the time scale of the step-cycle experiment, increases slower than the applied strain, for all samples. From this point on, the slopes of curves increase and eventually they become roughly parallel to the line representing a perfect plastic body.

It is also interesting to compare the magnitude of both cyclic and base strain components. It can be seen in Fig. 4(b) that in a highly crystalline sample of H-1 the permanent, base strain, e_{p0}, is higher than the recoverable, cyclic part of the strain, e_{r0}, from the very beginning of the deformation process and this difference increases steadily with an increasing applied strain. On the other hand, in the low crystalline sample of E-2, the recoverable part of the strain is higher than the permanent one in the initial stage of deformation. This changes only after saturation of the cyclic component, while the remaining (base) strain increases further with an increase of the applied strain. Both lines intersect around a relatively high true strain of $e=0.7$ (compression ratio of 2).

From the cyclic strain curves (Fig. 4(a)) the maximum recovered strain and the strain recovered at heavy deformation ('plateau' value) were determined and plotted as a function of the amorphous contribution in the sample.

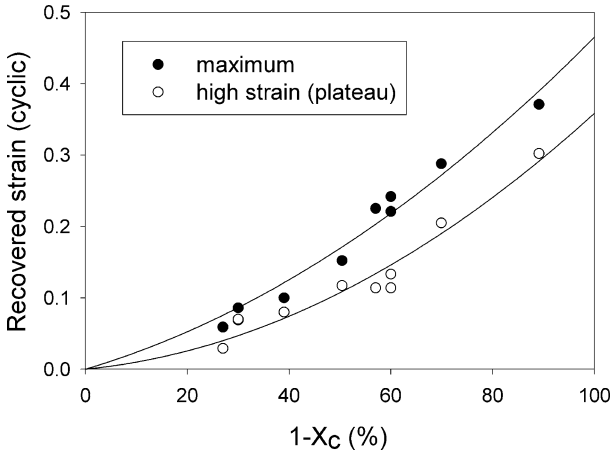

Fig. 5. The recovered (cyclic) strain, as measured in maximum and in the range of high strains, plotted against the amorphous fraction of the material.

This plot is presented in Fig. 5. It can be inferred from this plot that the recovery behavior of the material depends on the fraction of amorphous component. Moreover, the extrapolation to 0 (i.e. fully crystalline material) supports an obvious conclusion that the inelastic recovery process should cease completely then and such 100% crystalline material should respond as a nearly perfect plastic material. This demonstrates that except for a relatively small elastic contribution, the observed recovery is related entirely to the amorphous component.

Apart from the general dependence on the amorphous phase content, another trends can be found in the data shown in Fig. 4. First is a systematic shift of the maximum of the recovered strain toward higher applied strain with an increasing amount of the amorphous component (increasing monotonically from H-1 to E-2). This is especially well seen when comparing highly crystalline linear samples H-1 and H-2 exhibiting that maximum around $e=0.5$ with the samples of lower crystallinity, such as ultra-high molecular mass U-2 or branched polyethylenes and copolymers, all showing the maximum of recovered strain at the strain above $e=0.6$. That shift of the maximum is illustrated with broken lines in Fig. 4(a). Recently, Fu et al. [9] observed a similar evolution of the recovery behavior in the series of drawn samples of linear PE. Another trend can be found when comparing the recovery behavior of samples H-1, H-2 and H-5 or separately L-3 and L-5, which demonstrate comparable crystallinity and branching level within a group: The recovery is stronger in materials of higher molecular mass, exhibiting higher density of entanglements [22].

To analyze further the recovery behavior, it is useful to look back on plots of strain vs. stress, as those presented already in Fig. 3. Fig. 6 shows another, similar plot of the strain and its components as a function of stress, obtained for the E-1 copolymer.

Fig. 6(a) presents the data in the entire stress range, while Fig. 6(b) displays an enlarged initial part of the same curves. Very similar dependencies were found for other polymers

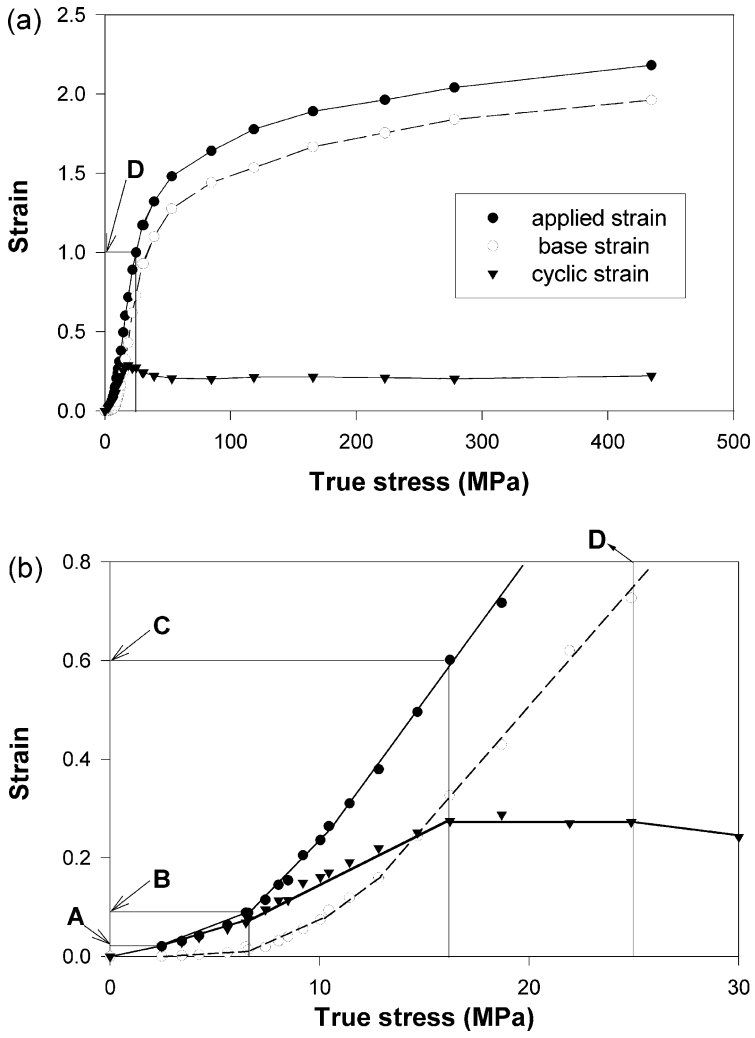

Fig. 6. Decomposition of the strain into recovered (cyclic) and remaining (base) components on the basis of the data collected in step-cycle recovery tests for sample of E-1 copolymer. Plot (b) is an enlarged view of initial stage of deformation process.

under investigation (cf. Fig. 3), so we limit the discussion to the example of sample E-1 presented here. To simplify the analysis, experimental dependencies can be approximated by several straight lines, drawn through data points. Then, one can observe on the curves shown in Fig. 6 that during deformation the sample passes through several different regions with crossovers at four specific points denoted by *A*–*D* (after Strobl et al. [6–11]). At the beginning of deformation, there is the range of the lowest strain and stress, extending up to point *A* (Fig. 6(b)). In this region the sample responds as an ideal elastic solid, with the linear stress–strain relationship and no permanent (base) strain ($e_{p0}=0$, $e_{r0}=e$). Passing point *A*, a finite base strain ($e_{p0}\neq 0$) starts to develop, and the differential compliance $de/d\sigma$ increases at the same time. The next change in material response can be found around point *B*. One can observe here a further, now quite pronounced, increase in the differential compliance. As demonstrated in Fig. 6(b), this increase is produced by both cyclic and base parts of the differential compliance ($de_{r0}/d\sigma$ and $de_{p0}/d\sigma$, respectively). With a further increase of the applied strain and associated stress, the base strain component continues to increase while the cyclic component levels up and reaches a plateau region. This can be marked as a next cross-over point, *C*. That plateau region of recovered (cyclic) component ends at the fourth characteristic point *D*, associated with a decrease in the cyclic component of the strain and further noticeable decrease of the differential compliance $de/d\sigma$. Point *D* coincides well with the onset of a strong strain hardening stage of the deformation process, observed in the stress–strain curve. Soon after passing that point (*D*), the recovered (cyclic) part of the strain reaches a new, final plateau and then its value remains constant up to the end of the deformation process (D' near the strain of $e=1.2$). The above four cross-over points *A*–*D* define five regions of different deformation behavior. They are located at the approximate strain of 0.02, 0.1, 0.6 and 1.0, respectively.

Comparing the data obtained for other samples, we found the same deformation scheme, as described above for the E-1 copolymer. Moreover, the cross-over points *A*–*D* were

located at almost the same respective strains for all materials studied, regardless of the developed stress. What is important, the same behavior, and the same location of cross-over points, were found previously in the range of polyethylenes and their copolymers when deformed in tensile mode [6–9]. The same scheme was also observed in tensile deformation of syndiotactic polypropylene [10] and isotactic polybutene-1 [11]. All these findings clearly demonstrate that the discussed scheme of deformation is of general nature, not specific for a particular semicrystalline polymer nor deformation mode, at least at temperatures of deformation above glass transition of respective polymers. Below T_g, when the amorphous component is glassy, its response to strain would be different, which in turn, could modify noticeably the deformation behavior.

The cross–over points *A*, *B*, *C* and *D* discussed above may also be identified in dependencies of recovered and base strains on applied strain, which were introduced in Fig. 4. Points *A* and *B* can be identified easily on enlarged plots. However, one can observe here a broad maximum of a recoverable strain component rather than plateau defining points *C* and *D*, as shown in Fig. 6. On the other hand, Fig. 4 demonstrates more precisely that the recovered strain after a decrease at the strain roughly above of 1.0 (point *D*) stabilizes and develops the final plateau in the range of applied strain of $e=1.2$–1.4. Therefore, the curves shown in Fig. 4 allow us to modify the two latter characteristic points: Maximum of the recovered strain, C', located at the strain around 0.6–0.7, and the onset of the final plateau, D', at $e=1.2$–1.4. These new points, replacing *C* and *D*, can refine the description of recovery behavior as compared to the original four-points scheme, proposed by Strobl et al. [6].

In the second set of recovery experiments we measured the dimensions of samples deformed to the pre-defined strain in a single step and then quickly unloaded and taken out from the channel-die in order to allow them to recover in an unconstrained way at room temperature. For these experiments large samples deformed in a deep channel-die were used. For comparison, the recovery behavior of selected samples deformed continuously in a small die as well as of samples from the step-cycle experiment described above was also checked out. We did not find any serious difference in the recovery behavior of respective samples deformed in a deep channel-die or in a small die either in a single run or deformed according to the step-cycle protocol.

It was found that all samples demonstrated strain recovery stronger than in the step-cycle experiment. This recovery was limited to the loading and flow directions only. As expected for plane-strain deformation the dimension measured along CD direction of every sample tested remained constant, even for a very long time after unloading (CD was the direction of external constraints imposed by the side walls of the channel). In contrast, dimensions measured along LD and FD varied substantially over a long period of time, even up to 1 month after unloading for some polymers (e.g. U-1, U-2).

Fig. 7(a) and (b) present dependencies of the recovered, e_{r1}, and remaining in the sample, e_{p1}, strain components on the applied strain, *e*. Both were calculated as true strain components based on measurements of a specimen dimension along the loading direction, LD, done 1 h after unloading. The inset in Fig. 7(b) shows the evolution of the remaining strain, e_r, with time for three representative samples of H-2, U-2 and E-2, deformed to the true strain of $e=1.0$. These curves demonstrate that the rate of strain recovery is a time-dependent process. Its rate is the highest in the initial stage of recovery: On specimen unloading and during the first few minutes after its withdrawal from the channel-die. After that initial period the recovery slows down gradually. Consequently, it is almost completed within the first hour after unloading, although ceases completely after the period between 2 weeks and 1 month. The strain recovered after sample unloading consists of two components: Instantaneous elastic strain, and time-dependent inelastic one. As demonstrated by the step-cycle test the elastic part does not exceed $e=0.02$ (point *A*, limiting proportionality range of the stress–strain curve). The major part of recovered strain is then of viscoelastic nature.

Comparing the results presented in Fig. 7 with respective results of the step-cycle experiment, shown in Fig. 4 one can see that the curves obtained in the free recovery and step-cycle experiments show similar features. The main difference is, however, in the amount of recovery, e.g. the maximum value of the recovered strain component for sample E-2 observed in the step-cycle test was $e_{r0}=0.37$, while in the free recovery test it was $e_{r1}=0.98$ (at 1 h); a similar increase of the recovered strain was observed also in other samples. Simultaneously, a shift of the maximum of recovery (point C') towards higher applied strains was observed. While for most samples that maximum shifted to approx. $e=0.8$, it shifted as far as to $e=1.5$ for E-2 copolymer. These observations can indicate that the higher the applied strain the longer the relaxation times of the strain recovery process.

Finally, in the third recovery experiment the samples deformed and then fully recovered at room temperature (at least 1 month after their deformation and unloading) were slowly heated up to the temperature close to their respective melting temperature and annealed at that temperature for 10 min. After cooling down, their final dimensions were measured and the recovered and remaining parts of the strain, e_{r2} and e_{p2}, respectively, were evaluated. Fig. 8 presents the results of this experiment. Annealing at the temperature near the melting point led to the highest possible strain recovery, so that only strain e_{p2}, remaining in the sample after such a thermal treatment can be considered as a truly permanent, irreversible plastic strain. Similarly to the results reported earlier, this permanent plastic strain increases with increasing crystallinity of the material. Moreover, again, as illustrated by samples L-3 and L-5 of comparable crystallinity (i.e. also the amount of amorphous component) and branching level, the permanent plastic

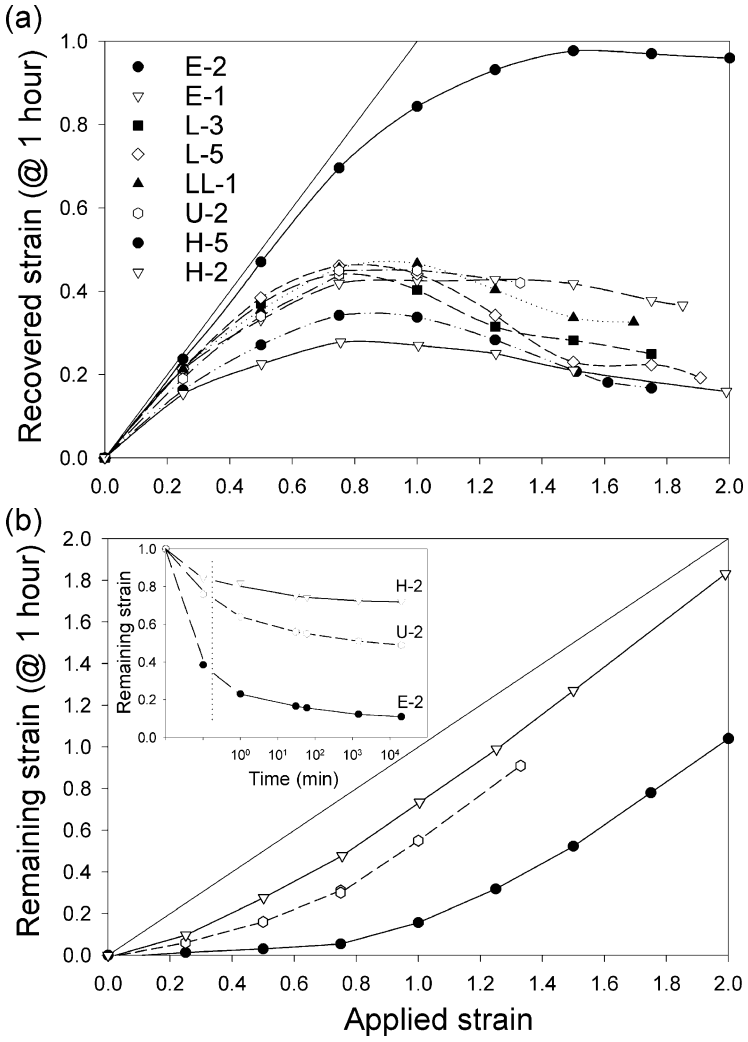

Fig. 7. Dependencies of recovered (a) and remaining strains (b) after 1 h of free recovery at room temperature on the applied strain for samples indicated in legend. For clarity only selected curves are presented in (b). Straight line of the unit slope in (a) illustrates an ideal elastic behavior, while that in (b) an ideal plastic behavior. Inset in (b) shows the time dependence of the strain recovery for samples H-2, U-2 and E-2 deformed to the true strain of $e=1.0$. Two first points on the left-side of the graph show the strain of loaded and unloaded, but still remaining inside a channel-die specimen, respectively. A dotted vertical line indicates the moment of taking the specimen out of the die.

strain is higher in materials of lower molecular mass, i.e. exhibiting smaller entanglement density. A new feature of the curves of e_{r2} and e_{p2} is the modification of their shape comparing to the respective curves observed in partial recovery tests at room temperature (both short-term in cyclic experiment, e_{r0}, e_{p0}, and long-term in free recovery tests, e_{r1}, e_{p1}). While in samples of high crystallinity (linear homopolymers) the maximum of the recovered strain is preserved (although shifted again to even higher strains, now around $e=1.0$, and not followed by the final plateau region at the high strain side), the situation changes in samples of crystallinity below 50 wt%. In these samples the maximum in the recovered strain is no longer observed and e_{r2} increases steadily with an increasing initial strain. At the strain near $e=1.0$ only a change in the slope of e_{r2} curve can be noticed (for all samples). Interestingly, in samples of low crystallinity, like E-2 copolymer, the strain below 1 appeared completely reversible and no permanent deformation was detected (cf. Fig. 8(b)). The permanent strain starts to develop only for a higher applied strain. This transition near $e=1$ is another clear mark of the point D of Strobl's deformation scheme.

3.2. Changes of lamellar structure induced by deformation

The orientation behavior and texture evolution of the studied materials is discussed in detail in a separate paper [26]. Here only some structural changes will be described, particularly those associated with the characteristic point C', ascribed to a maximum of the fast recovery, located near the strain of 0.7, and point D', indicating the plateau of final, lowered recovery strain, situated in the range of $e=1.2$–1.4. Fig. 9 shows two-dimensional small-angle X-Ray scattering patterns, obtained for samples of H-2 and L-5, deformed to

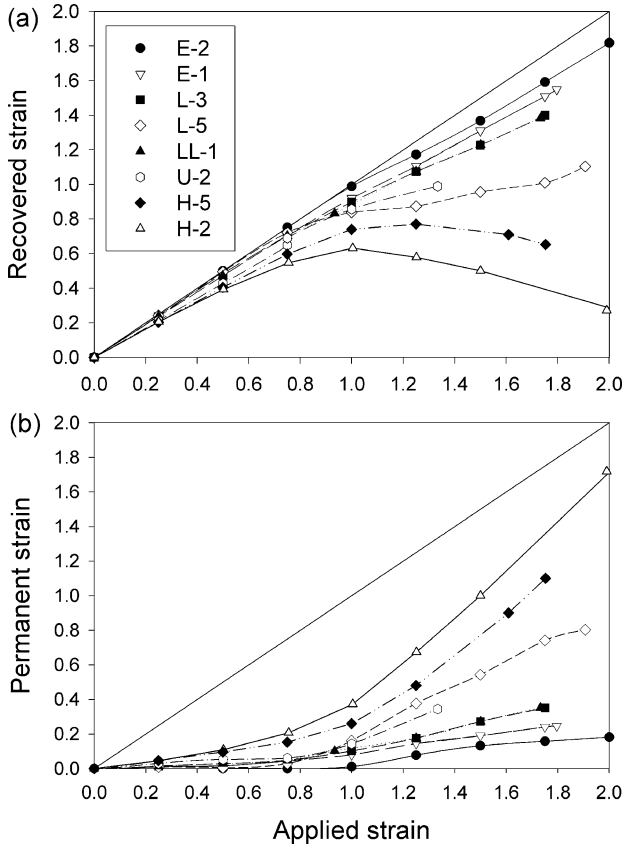

Fig. 8. Dependencies of recovered (a) and remaining strains (b) after free recovery at the temperature approaching the melting point of the respective polymer on the applied strain for samples indicated in legend. Straight line of the unit slope in (a) illustrates an ideal elastic behavior, while that in (b) an ideal plastic behavior.

the strain of $e=0.75$ and to $e=1.25$, i.e. close to points C' and D'. In samples deformed to $e=0.75$ (patterns (a) and (b)) the four point signature can be found for the first time. This feature was not observed in the samples deformed to lower strains. That four-point signature, developing further in the samples of higher deformation, indicates the formation of two well-defined populations of lamellae, both oriented at some acute angle with respect to the flow direction. This is an indication of the onset of lamellae fragmentation, although very limited at this stage, due to cooperative kinking of some stacked lamellae oriented initially with their normals roughly perpendicular to the loading direction, LD. That specific orientation should promote kinking process [27]. The fragmentation of lamellae produced by kinks is very limited, since lamellae break then in no more than few points along their length. Moreover, only a fraction of lamellae population (i.e. only those oriented accordingly) undergoes kinking.

The evidence of the lamellae kinking is given by transmission electron microscopy. Fig. 10 demonstrates a TEM micrograph of sample H-1 deformed to the strain of 0.8, in which the cooperative kink of the stacked lamellae can be clearly observed.

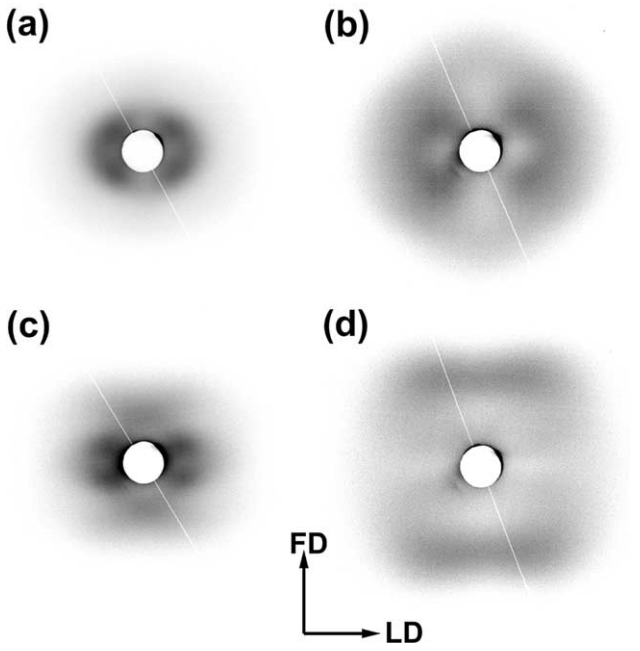

Fig. 9. Two-dimensional SAXS patterns recorded for samples of linear PE H-2 deformed to the true strain of 0.75 (a) and 1.25 (c) and branched L-2 deformed to the same strains ((b) and (d), respectively). Vertical direction in patterns coincides with the flow direction (FD), while horizontal with the loading direction (LD).

In the SAXS pattern obtained for H-2 sample deformed to $e=1.25$ (Fig. 9(c)) the four-point signature, observed in the samples of lower strains, was gradually replaced by another one consisting of two lines, both perpendicular to the flow direction, FD. This can be an indication of the destruction of the existing lamellar structure by stronger fragmentation and its restructurization into a new one, consisting of smaller lamellar blocks, all oriented with normals approximately along FD [25,26,28,29]. This new

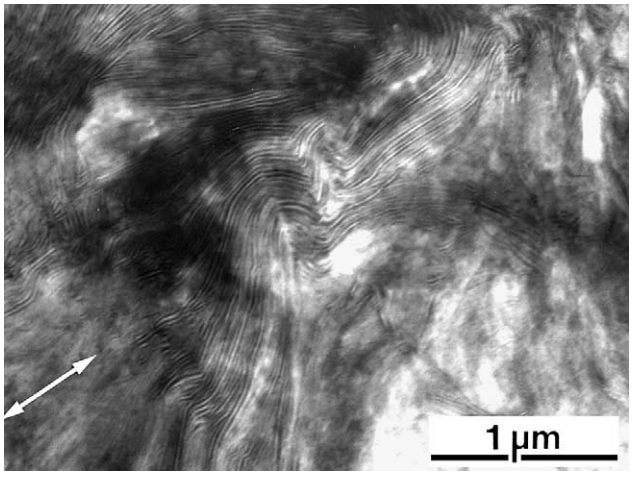

Fig. 10. Transmission electron micrograph of ultra-thin section of H-1 linear homopolymer deformed to the true strain of 0.8. The material was stained with chlorosulfonic acid prior to sectioning. Arrow on micrograph indicates the direction of loading (LD). Direction of flow is perpendicular to LD in the plane of section.

orientation component produces a new long period observed in FD along with traces of oriented old lamellar structure, not completely destroyed yet. For higher strains the four-point signature of old structure dissolves completely and only a new long period can be seen. Such an advanced destruction of the lamellar structure happens at high strains, well above 1.2, although it is limited to samples of relatively low molecular mass, as H-1 or H-2, discussed above ($M_w < 10^5$). Samples of higher molecular mass do not undergo such an intense lamellae fragmentation in plane-strain compression and their SAXS patterns demonstrate the four-point signature even at high strains [26]. Similar conclusions concerning transformations of the lamellar structure at advanced strain were drawn from our previous studies of the plastic deformation of polyethylene [25,27,30]. Particularly, the destruction of the lamellar structure and its restructurization into a new structure was investigated in detail in Ref. [25]. It was found then that such a transformation took place in HDPE (equivalent to H-1, studied here) at the compression ratio near 3.1, i.e. the true strain near $e = 1.14$. Similar transformation, known as fibrillation, is commonly observed in tensile deformation. It was attributed to the change of the mode crystallographic intralamellar slip from homogeneous slip to highly localized heterogeneous (coarse) slip [29,31].

4. Discussion

Results presented in Section 3 confirm the general deformation scheme proposed recently by Strobl et al. on the basis of tensile experiments [6–11]. It is evident that this scheme is valid also for other deformation modes, as the plane-strain compression implemented in this study, or uniaxial compression studied in the past [27]. This scheme emphasizes the role of the amorphous component with its topological structure consisting numerous entanglement of chains as well as tie-molecules connecting two adjacent crystals with the amorphous region in between. Although both tie-molecules, connecting directly neighboring lamellae, and entangled chains anchored on the crystal–amorphous interface also providing connectivity of phases seem to be equally important structure elements, their amount within amorphous phase is very different. The fraction of tie-molecules in samples of melt crystallized linear polyethylene was found to be dependent on molecular weight, crystal sizes and overall crystallinity and was estimated usually at the level of 1–3% [4,5,32], although some researchers estimated the probability of formation of a tie molecule as high as much above 20% [33,34]. It means that only a relative small fraction of chains can form tie-molecules. On contrary, chain entanglements are much more frequent features. The average molecular mass of the chain segment between entanglements was estimated for PE melt as 1240 g/mol [35]. Most of these entanglements cannot be resolved during rapid crystallization (as employed in this study) but become rather concentrated in the form of entangled loops within amorphous layers [36]. In the companion paper [22] an average length between entanglements within amorphous phase of fast-crystallized polyethylenes was estimated to be 400–1300 g/mol, depending on the molecular mass and architecture of the chain (corresponding density of entanglements $N_e = 4–12 \times 10^{26}\ m^{-3}$). This means that every macromolecule contributes to numerous entanglements: From a few in low molecular weight PE of high crystallinity, like H-1, up to several hundreds in PE of high molecular weight, like U-2. This demonstrates that chain entanglements are much more frequent features than classical tie-molecules, therefore, the properties of an amorphous phase and its performance should depend primarily on the network of entangled chains. Nevertheless, as it will be discussed later, the tie-molecules, although less numerous than the bridges formed by entangled chains, play also very important role at some stages of the deformation sequence.

It is apparent that the elastic region of deformation is limited to the low strain range of the true strain below $e = 0.02–0.03$ (point A). At this point the linearity is lost and a plastic deformation by crystallographic slip and interlamellar shear of the amorphous layers starts to develop, which is indicated by a small long-living strain component e_{p1}. As suggested by Strobl et al. [6], the deformation is probably limited spatially to the isolated microdomains around those lamellae already oriented to produce the highest resolved shear stress in the given stress field, approaching critical values for particulate slip systems. It was found that the easiest slip system in polyethylene, (100) [001] chain slip system, can be activated by the resolved shear stress as low as 7.2 MPa [30] (that value was obtained for highly crystalline linear PE, H-1; even lower values can be expected in the samples consisting of thinner crystals [37–39]), while the interlamellar shear of amorphous layers can happen for even smaller shear stress [27]. The deformations within separated microdomains develops and their number multiplies with strain and stress increase up to the point B, at the true strain of approximately 0.1, around which the mutual stabilization against the elastic back-stress of the not-deformed-yet surroundings and eventual coalescence of the growing domains of active shear deformation takes place. This leads to a cooperative action and brings an onset of the macroscopic flow behavior, i.e. a macroscopic yield point is reached. From the microscopic standpoint, yielding begins when the concentration of mobile dislocations reaches the critical level for activation of a given slip system [2,3]. Such a two-stage description of the process is quite similar to that proposed for yielding of amorphous polymers, where deformation is assumed to begin with shear within isolated microdomains, and to develop through their multiplication and stabilization, which results in a cooperative action and a macroscopic plastic flow.

It can be noted that the macroscopic yield point commonly defined by a local maximum on the load-

elongation curve, or by an alternative offset definition (in the absence of load maximum, as in the compression curves analyzed in the companion paper [22]), coincides quite well with the strain characteristic of the cross-over point B, at which the differential compliance increases noticeably and a non-recoverable strain component appears for the first time. The results presented in Part I of this study [22] and in this paper evidence very well this correspondence.

As pointed out above, the yielding is governed primarily by deformation of the crystalline component through the activation of crystallographic slips. Rubber like amorphous layers, being highly compliant, yet intimately connected to adjacent crystals through numerous chains crossing crystal–amorphous interface and, therefore, highly constrained by these crystals, have a slight effect on yielding. They participate in the macroplasticity in this strain range only owing to the stress transfer from one lamella to another [12] and strain accommodation. This view is strongly supported by the observed dependence of the yield stress on lamellar thickness [22] evidencing that the yield stress is controlled by the nucleation of dislocations, being the principal elementary carriers of plastic deformation in crystals at the microscopic level.

Further deformation after passing point B proceeds by intense crystallographic slips supported by interlamellar shear, necessary to substitute the lacking independent slip systems in order to accommodate an increasing strain (generally the activity of five independent slips is necessary to produce an arbitrary change of the shape of a solid; in polyethylene there are only three active basic slip systems, all operating in planes parallel to the chain direction [1–3, 30]). While the deformation of crystalline component is predominately plastic, the accompanying interlamellar shear of amorphous layers can be partially reversible due to the presence of the network formed by entanglements and these molecules, which are fixed to the adjacent crystals, like tie molecules of fixed length. The retractive forces resulting in sample recovery originate primarily from shearing of this network. The role of tie-molecules is limited at this stage since they are not fully stretched yet. They contribute to the network in similar way as other chain segments immobilized by entanglements. The deformation proceeds according to these mechanisms up to the strain of the next cross-over point C. It was postulated that the change of the deformation behavior beyond this strain was associated with an intense fragmentation of lamellae and formation of fibrils [6,7,29].

The fibrillation transformation, while frequently seen in tension [29], is not observed in compression due to substantial differences in the stress field in compression and tension. The stress distribution in the plane-strain compression, especially in the presence of compressive components along LD and CD, produces additional constraints and inhibits a massive fibrillation of the material, which is commonly observed in a less constrained tensile deformation. Nevertheless, the transition point C (or alternatively C', at $e=0.6$–0.7, characterizing better the deformation scheme) is observed at the same strain range in both tension and compression. In our previous studies [27] we have found that in this range of the applied strain the intense lamellar shear comes to the extensibility limit and 'locks'. At this stage some segments between points defining the amorphous network (i.e. those anchored in adjacent crystallites, like tie-molecules, or cilia and long loops immobilized by tighened knots of entanglements) become fully stretched out, so any further deformation of the amorphous layers by their shear becomes extremely difficult. That lock of the amorphous shear leads to saturation of the recoverable strain and consequently to formation of a local maximum in the recovery response at point C' ($e\sim0.6$–0.7). Due to the presence of the fully stretched tie-molecules, the stress increases rapidly and is transmitted easily to the adjacent crystallites, which in turn, causes intensification of the crystallographic slip, supposedly with its localization due to stress concentration around tie molecules. Such a localization leads shortly to partial destruction of the lamellar structure, which implicates also some topological changes of the amorphous network in the vicinity of lamella breaks. This step is inevitable because the termination of the interlamellar shear would otherwise limit or even terminate the deformation of crystallites by crystallographic slips since both components are still intimately connected by strong covalent bonds and have to deform simultaneously and cooperatively. In a much less constrained tensile deformation, heavy localization of the slip results in the beginning of a massive fibrillation process. However, when constraints are stronger, as in the compression mode, only a quite limited destruction of lamellae, manifesting itself in the formation of lamellar kinks, is possible. This is evidenced by SAXS and TEM (cf. Figs. 9 and 10). Nevertheless, even such a limited destruction of lamellae as that resulting from kinking leads to a substantial change of the local orientation, which in turn would allow further intense plastic deformation of reoriented crystallites by slip systems. Simultaneously, the formation of kinks relieves some of the constraints from the amorphous component, possibly reducing the ultimate stretch of tie-molecules and other immobilized and highly strained segments of the network. so that the interlamellar shear 'unlocks' for a while and can proceed further to accompany deformation of the crystalline component by slip mechanism.

As it was already mentioned in Section 3, the point C' (maximum of the recovered strain) shifts systematically toward higher applied strain with increasing amount of the amorphous component in the sample. This is especially well seen when comparing highly crystalline linear samples H-1 and H-2 that exhibit this maximum around $e=0.5$ with the samples of lower crystallinity, such as the sample of ultra-high molecular mass U-2 or samples of branched polyethylenes and copolymers, all showing the maximum

of recovered strain at the strain above $e=0.6$ (this shift is illustrated with a broken line in Fig. 4(a)).

Recently Fu et al. [9] discussed similar evolution of the critical strain characteristic for the point C in a series of drawn samples of linear PE. They found this critical strain dependent on the thickness of the amorphous layer between crystalline lamellae: Samples with amorphous layers thinner than approx. 6 nm demonstrated the critical strain C below $e=0.4$, while these in which amorphous layers were thicker than 6 nm demonstrated the critical strain C near $e=0.6$. Such a behavior was interpreted in terms of changes of the local entanglements density within amorphous layers with decreasing thickness of these layers, due to rejection of numerous entanglements into the amorphous layers during crystallization, which resulted in a reduction of chain mobility. A further reduction of their mobility should arise from immobilization of these chains, which cross crystal–amorphous interfaces (tie molecules, cilia, etc.). Consequently, the stiffness of the molecular network within the amorphous layers of decreasing thickness should increase considerably. On that basis the shift of point C towards lower strain was anticipated for highly crystalline samples with thin amorphous layers [9].

Our results do not support such explanation, since the density of entanglements and resulting stiffness of the molecular network in high molecular weight samples, as, e.g. U-1 or U-2 ($G_n \sim 5$ MPa), is considerably higher than that of lower molecular weight, yet highly crystalline samples H-1 to H-3 ($G_n \sim 2$ MPa) [22], in which a part of entanglements pre-existed in the melt was able to resolve by reeling in of short chains to growing crystals [40]. These low molecular weight linear polyethylenes exhibit quite thin amorphous layers (7 nm) of relatively low stiffness, yet the critical strain C is lower than in U-1 or U-2 containing considerably stiffer amorphous component. In our opinion, that shift of cross-over point C towards lower strain can be due to an increasing relative contribution of tie-molecules to the molecular network of highly crystalline low molecular weight samples. The number of tie molecules tends to increase with increasing molecular weight and decreasing thickness of lamellae [4,5], therefore, it is expected to be higher in U-1 or U-2 than in H-1 to H-3 samples. However, the rough estimations based on the equation proposed by Huang and Brown (3a,b) done for linear PE's used in this study (data of the thickness of crystalline and amorphous layers were taken from Ref. [22]) demonstrated only a moderate increase of tie molecules fraction by approximately 1/3 when going from H-1 to U-2. On the other hand, the number of entanglements in the amorphous component also increases, yet much stronger—estimated entanglement density in U-2 is nearly three times higher than in H-1 [22]. Therefore, the contribution of tie molecules to the network relative to that of entanglements is most probably higher in H-1 (low molecular weight, high crystallinity) as compared to U-2 (high molecular weight and moderate crystallinity).

The tie molecules consist of relatively short sequences immobilized on both sides of the narrow amorphous layer by adjacent lamellae. These chain fragments are constrained more than other chains participating in the molecular network through mobile entanglements. Consequently, the tie molecules exhibit an extensibility limit lower than other chains of the network cross-linked by mobile entanglements and would stretch out completely relatively early. This can result in an earlier 'locking' of the deformation of such amorphous layers in which the relative fraction of tie molecules in the network is increased, and in local stress build-up at amorphous–crystal interfaces at many points where those tie-molecules cross the interface. The stress concentrations produced by fully stretched tie molecules would in turn lead soon to localization of the deformation of crystals and their probable fragmentation. Since the relative contribution of tie-molecules in the molecular network within the amorphous layers seem to increase with increasing crystallinity and accompanying reduction of the thickness of these layers within the set of samples studied, the cross-over point C (C') in highly crystalline samples like H-1 might be expected at lower strains than in other with higher molecular weight and thicker amorphous layers, in which the network is expected to have larger contribution of entanglements.

In compression, the destruction of lamellar structure, beginning with a quite limited fragmentation due to kinks formation at strains around point C', must go further with the increasing strain, because the interlamellar amorphous layers relieved from constraints for a moment (although only to a certain limited extent) and then sheared again have to 'lock' soon once more. This should lead to a more extensive fragmentation of the lamellar structure into smaller blocks. Such a transformation was in fact observed in compression at the strain above of 1.1 [25,26], but only in the samples of relatively low molecular mass ($M_w < 10^5$) and high crystallinity, most probably featuring relative high fraction of non-resolvable intercrystalline links (tie-molecules, tight entanglement knots of chain segments participating in adjacent crystallites) [26]. At some stage of deformation, the interlamellar shear accompanying the deformation of crystallites by slip leads to full extension of these links. This in turn results in constraining the slip process and its strong localization due to stress concentrations at the points of entering tie molecules into crystals. As a consequence of such localization, lamellae soon undergo fragmentation. This transformation is more massive than the limited fragmentation observed earlier, near point C, since most of crystals are already oriented and seriously thinned due to previous slip activity [25]. However, in the samples of higher molecular mass with a higher contribution of mobile entanglements in the amorphous network, such a process of lamellae destruction is much less intense and probably postponed to the region of higher strain since many of intercrystalline links are produced by entangled chains, which can be resolved by shear. This allows for a further advance of both

homogeneous chain slip and associated shear of inter-lamellar layers with only a minor slip localization and associated destruction of the lamellar structure.

The change of slip mode from homogeneous to heterogeneous due to its localization and resulting fragmentation of lamellar structure was also studied in the past by Gaucher-Miri et al. [29,31]. They concluded that both slip modes have different strain hardening rates in relation to the different ways of straining of chain folds. The homogeneous slip is usually preferred to initiate the plastic flow, especially at low strain rate or high temperature and for thinner crystals. However, as the strain increases, its high strain hardening makes it less favorable than heterogeneous slip of lower strain hardening, which turns gradually active in place of homogeneous slip [29]. It seems that the mechanisms of lamellea fragmentation proposed in this paper and by Gaucher-Miri et al., although emphasis slightly different aspects of the process, do not contradict each to the other.

At strains above 1 (after passing point D) the stresses, generated by deformation of the network of amorphous entangled chains, strained now again nearly up to the extensibility limit of the entire network, become high enough to induce disentanglements of some entangled chains. Note, that tie molecules, stretch of which triggered transition at point C, became at least partially released by the lamellae fragmentation, discussed above (possibly by some unwinding from the broken crystals), so that they do not constrain the entangled network as much as before. Such disentanglement leads to a gradual erosion of the molecular network through the change of its topology. Consequently, the memory of the undeformed macro-state can be progressively erased. At this point, a truly irreversible deformation of the amorphous component is initiated. The process of resolution of chain entanglements leads to an additional relaxation of the network, manifesting itself in a decrease of the recovered strain component at high applied strains (the final plateau region beyond point D', observed in the step-cycle as well as in 'free' room temperature recovery tests; cf. Figs. 4 and 7). The irreversibility of that deformation part associated with erosion of the network of entangled chains is evidenced by results of the recovery experiment performed near the melting point, presented in Fig. 8. These data indicate that the permanent strain left after annealing increases steadily with an increasing strain applied, yet with significant acceleration above the applied strain of $e=1.0$. It can be reasoned that the permanent strain at the applied strain below 1.0 results primarily from a permanent plastic deformation of crystallites (note that it almost disappears in the samples of very low crystallinity, as E-1 or E-2 copolymers). However, at higher strains apparently the new mechanism sets in, leading to a substantial increase of the permanent, truly irreversible component of the strain. This mechanism must be the deterioration of the molecular network, most probably through the resolution of chain entanglements, since a considerable fraction of the deformation achieved above the applied strain of $e=1$ remains in the sample even after melting of the crystalline phase. Another possible source of the postulated network deterioration may be also the scission of the most strained chains immobilized by interfaces or tightened entanglement knots.

The recovery behavior clearly illustrates that there had to be a truly irreversible plastic flow of the amorphous chains during the advanced stages of the deformation process, which led to the noticeable change of the chain distribution and topology of the molecular network in the highly deformed sample. The above explanation can be additionally supported by the results of model calculations reported in Part I [22]. At the strain well above 1, the calculated stress–strain curves demonstrated much stronger strain hardening than the curves obtained experimentally (cf. Fig. 7 in Ref. [22]). That dramatic rise of predicted stress with increasing strain is due to approaching of extensibility limit of the molecular network. The less intense strain hardening observed in experimental curves above $e=1.4$ as compared to calculated ones, can suggest the network evolution postulated above.

There is a variation in the network deterioration (disentangling) process with a change of molecular weight and chain architecture of a polymer (long- and short branching) as well as crystallinity due to different properties of the entanglements network. The variation of network properties leads to different levels of erosion of the network at high strains and, therefore, also to the variation in strain recovery behavior. Larger strain recovery is observed in final stages of the deformation of samples with higher molecular mass or higher branching, i.e. those demonstrating higher density of entanglements [22]. This can be explained by the fact that long molecules could resolve entanglements on much longer time scale than shorter chains can do. This time can also be longer than the time scale of the deformation experiment. Therefore, a larger amount of recoverable strain energy is stored by trapped entanglements in the network of long and/or branched chains as compared to the network formed by shorter, linear chains, which can erode by resolution of entanglements at the advanced deformation stage much more easily.

Results of this study as well as previous research of Strobl et al. [6–11] may suggest that the entire deformation process is strain-controlled and the sequence of the well defined events as well as the strains at which they happen are practically invariant, depending only a little on the molecular parameters of particular polymer samples. This is likely in the case of two transitions taking place at strains described by points C and D, both related to deformation of the network of entangled chains in the amorphous component, which undergoes some topological modifications when stretched up to the extensibility limit. Apparently, the differences in properties of molecular networks formed in various semicrystalline samples [22] are not large enough to give a substantial variation of critical

strains for the transformation observed in points *C* and *D*, so that both appear as nearly invariant.

The strain control over points *A* and *B* of the deformation scheme, although suggested by the strain recovery data, can be disputed. These points describe the activation of plastic deformation processes occurring in crystalline part of the sample (on the local scale in point *A* and globally in *B*), which are governed by deformation mechanisms of entirely crystallographic nature, known to be controlled by the resolved shear stress. In our opinion, the observed invariance of the strain at these transition points *A* and *B* can be merely a side-effect of structural differences of the samples studied (like the length of crystalline stem, overall crystallinity, small variations of unit cell dimensions or various supermolecular structures), which tune up the critical stress for activation of appropriate crystallographic slip in particular samples. The observed strain invariance of the beginning of plastic deformation of various samples must be apparent, merely coinciding with the material response according to modified, structure-related critical resolved shear stress.

5. Conclusions

Results reported in a companion paper [22] and in this study confirm that the deformation behavior at low strains, including the yield range, is governed by the crystalline phase, while the role of the amorphous component at this stage of deformation is limited to transfer of the load to and between crystallites. This changes at higher strains, when the stresses generated by stretching of the network of entangled chains within sheared amorphous layers become higher than those accompanying deformation of the crystalline component, which eventually leads to the strain hardening.

Apart of a small elastic component, the deformation of crystalline phase is the irreversible plastic deformation, while the deformation of the amorphous phase appears partially reversible. The post-deformation time-dependent strain recovery was found to be related exclusively to the amorphous part. The recovered strain depends on the amount of amorphous component and properties of the network of entangled chains: It increases with an increasing fraction of amorphous part as well as with increasing cross-link density of the molecular network. The process is modified by tie molecules, contributing to the network and providing additional strong constraints for its deformation. Their influence depends on their contribution to the network relative to that of entangled chains, and depends on chain architecture, molecular weight, as well as size and amount of lamellar crystals.

The obtained results allow us to confirm the general deformation scheme proposed recently by Strobl for semicrystalline polymers deformed in tension [6–11]. Our results demonstrate quite convincingly that this scheme is valid not only in the tensile but also in compression deformation mode. However, an interpretation of the transition point *C*, ascribed by Strobl to the fragmentation of lamellar crystals and formation of fibrils should be modified. Our results suggest that the origin of this transformation is locking of the interlamellar shear of the amorphous layers due to ultimate extension of tie molecules, which leads to stress build-up and consequently to localization of crystallographic slip, which results in some destruction of the lamellar structure. While in the less constrained conditions of the tensile deformation this actually leads to a widespread destruction of the existing lamellar structure and formation of microfibrils, in compression experiments, where much stronger deformation constraints are present, it results merely in a very limited fragmentation by cooperative kinking of stacked lamellae. A more advanced destruction of lamellar structure can happen later, at higher strains, well above 1.2, although only in the samples of relatively low molecular mass. Samples of higher molecular mass do not undergo such an intense process of lamellae fragmentation in compression even at high strain. Both lamellar kinks or more advanced destruction of lamellar structure lead to a substantial reorientation of crystallites to favor chain slip advance as well as to some modification of the topology of the entangled network in adjacent amorphous layers, which relieves temporarily some of the deformation constraints. These phenomena allow for further accommodation of the strain by easy chain slip in the crystalline lamellae and accompanying shear of interlamellar amorphous layers.

To produce a truly irreversible deformation of semicrystalline polyethylene it is necessary to deform it to the strain of at least $e=1.0$ (point *D* of Strobl's deformation scheme). Before that point, nearly all strain related to the deformation of amorphous part can be recovered either by prolonged storage or annealing at high temperature. However, with an increasing strain the stress generated by stretching of the entanglement network becomes high enough to modify that network. Consequently, at the strain of above $e=1.0$–1.2 a gradual dissolution of the network of entangled chains in the amorphous component by resolution of some of chain entanglements sets in. This leads to a permanent, irreversible plastic flow of the amorphous component in addition to irreversible plastic deformation of the crystalline component and consequently to the erasure of the 'memory' of the undeformed macro-state of the material.

Acknowledgements

Grant 7 T08E 036 19 from the State Agency for Scientific Research of Poland is acknowledged for partial financial support of this work.

References

[1] Bowden PB, Young R. J Mater Sci 1974;9:2034–51.
[2] Lin L, Argon AS. J Mater Sci 1994;29:294–323.
[3] Oleinik EF. Polymer Sci Ser C 2003;45:17–117.
[4] Brown N, Ward IM. J Mater Sci 1983;18:1405–20.
[5] Huang YL, Brown N. J Mater Sci 1988;23:3648–55.
[6] Hiss R, Hobeika S, Lynn C, Strobl G. Macromolecules 1999;32: 4390–403.
[7] Hobeika S, Men Y, Strobl G. Macromolecules 2000;33:1827–33.
[8] Fu Q, Men Y, Strobl G. Polymer 2003;44:1927–33.
[9] Fu Q, Men Y, Strobl G. Polymer 2003;44:1941–7.
[10] Men Y, Strobl G. J Macromol Sci Phys 2001;B40:775–96.
[11] Al-Hussein M, Strobl G. Macromolecules 2002;35:8515–20.
[12] Seguela R, Darras O. J Mater Sci 1994;29:5342–7.
[13] Lee BJ, Argon AS, Parks DM, Ahzi A, Bartczak Z. Polymer 1993;34: 3555–75.
[14] Park JB, Uhlmann DR. J Appl Phys 1970;41:2928–35.
[15] Park JB, Uhlmann DR. J Appl Phys 1973;42:3800–5.
[16] Park JB, Uhlmann DR. J Appl Phys 1973;44:201–6.
[17] Tanaka N. J Therm Anal 1996;46:1021–31.
[18] Charoensirisomboon P, Saito H, Inoue T, Oishi Y, Mori K. Polymer 1998;39:2089–93.
[19] Pegoretti A, Guardini A, Migliaresi C, Ricco T. Polymer 2000;41: 1857–64.
[20] Pegoretti A, Guardini A, Migliaresi C, Ricco T. J Appl Polym Sci 2000;78:1664–770.
[21] Ricco T, Pegoretti A. J Polym Sci, Part B: Polym Phys 2001;40: 236–43.
[22] Bartczak Z, Kozanecki M. Polymer 2005;46:8210–21.
[23] Kanig G. Kolloid ZZ Polym 1973;251:782–3.
[24] Young RJ, Bowden PB, Ritchie JM, Rider JG. J Mater Sci 1973;8: 23–36.
[25] Galeski A, Bartczak Z, Argon AS, Cohen RE. Macromolecules 1992; 25:5705–18.
[26] Bartczak Z, Lezak E. Polymer 2005;46:6050–63.
[27] Bartczak Z, Cohen RE, Argon AS. Macromolecules 1992;25: 4692–704.
[28] Song HH, Argon AS, Cohen RE. Macromolecules 1990;23:870–6.
[29] Gaucher-Miri V, Seguela R. Macromolecules 1997;30:1158–67.
[30] Bartczak Z, Argon AS, Cohen RE. Macromolecules 1992;25: 5036–53.
[31] Gaucher-Miri V, Elkoun S, Seguela R. Polym Eng Sci 1997;37: 1672–83.
[32] Yeh JT, Runt J. J Polym Sci, Part B: Polym Phys Ed 1991;29:371–88.
[33] Nitta K-H, Takayanagi M. J Polym Sci, Part B: Polym Phys Ed 1999; 37:357–68.
[34] Hosoda S, Uemura A. Polymer J 1992;24:939–49.
[35] Pearson DS, Fetters LJ, Graessley WW, Strate GV, von Meerwall E. Macromolecules 1994;27:711–9.
[36] Flory PJ, Yoon DY. Nature 1978;272:226–9.
[37] Young RJ. Mater Forum 1988;11:210–8.
[38] Crist B. Polym Commun 1989;30:69–71.
[39] Brooks NWJ, Mukhtar M. Polymer 2000;41:1475–80.
[40] Hoffmann JD, Guttman CM, DiMarzio EA. Faraday Discuss ChemSoc 1979;68:177–97.